Scripta Materialia 138 (2017) 6–11

Contents lists available at ScienceDirect

Scripta Materialia

journal homepage: www.elsevier.com/locate/scriptamat

Regular article

On the prediction of martensite formation in metals

E.I. Galindo-Nava

Department of Materials Science and Metallurgy, University of Cambridge, 27 Charles Babbage Rd., Cambridge CB3 0FS, UK

ARTICLE INFO

Article history:
Received 29 March 2017
Received in revised form 9 May 2017
Accepted 17 May 2017
Available online xxxx

Keywords:
Martensitic phase transformation
Martensitic steels
Shape memory alloys
Titanium alloys
CALPHAD

ABSTRACT

A new approach to predict athermal martensite formation in metals is presented. It is based on computing the driving force of the transformation including a strain energy term induced by atomic shear displacements and energy terms due to substitutional and interstitial lattice distortions. The model is applied to prescribe the martensite and austenite start temperatures in Fe-, Ti- and Co-based alloys with no adjustable parameters. Expressions for M_s variations with composition are derived for multicomponent systems. The transformation temperature hysteresis is predicted in Co alloys showing that this approximation can be used to design alloys with the shape memory effect.

Martensitic transformations have been studied extensively due to their importance in applications for high-strength, shape-memory effects or superelastic properties. These are diffusionless first order solid-state transformations, which nucleate from a parent phase, commonly referred to as austenite. Martensite nucleates at a critical temperature M_s (martensite-start) when the driving force for its nucleation is reached. Additional undercooling is required for the transformation to continue and reach completion at a temperature M_f (martensite-finish). The reverse transition occurs upon heating the martensite to transform back to austenite; the temperatures at which the transformation begins and finish are austenite start (A_s) and finish (A_f), respectively. Although there are considerable studies in different alloying systems showing how martensite formation changes with composition [1–4], there is virtually no theoretical approximation able to predict the conditions for its occurrence without introducing fitting parameters or remaining valid in different phase transitions.

The objective of this work is to introduce a new approach to predict M_s in systems undergoing the phase transitions: face-centred cubic (FCC)⟺body-centred cubic (BCC), FCC⟺hexagonal closed packed (HCP) and BCC⇒HCP. The approach is based on determining the driving force for athermal martensite formation including energy terms of the transformation strains and lattice distortions by substitutional and interstitial atoms. The model has no adjustable parameters and it is able to predict M_s and A_s in Fe-, Ti-based alloys, as well as the hysteresis cycle (M_s, M_f, A_s, A_f) in Co-based alloys.

Martensite forms by the coordinated movement of atoms resulting in homogeneous shearing of the austenite and forming a new crystal structure without variations in chemical composition. The lattice correspondence between the austenite and martensite phases are nearly parallel to the most densely packed planes and their corresponding directions. This leads to the orientation relationships between the FCC, BCC, and HCP phase transitions to be[1]: $\{111\}_{FCC}||\{110\}_{BCC}||\{0001\}_{HCP}$ and $\langle 110\rangle_{FCC}||\langle 111\rangle_{BCC}||\langle 11\bar{2}0\rangle_{HCP}$.

The phenomenological theory of martensite crystallography dictates that the transformation strain γ_T consists of two components; a (Bain) strain distorting homogeneously the parent structure, and a lattice invariant strain δ aiding in producing the correct shape of the martensitic structure. For the FCC⇒BCC transition the transformation strain is computed by rotating the FCC unit cell, expanding two principal axes and compressing the remaining axis to correspond with the BCC unit cell [8]. Additional shearing of $\delta = \frac{|\sqrt{2}a_\gamma - \sqrt{3}a_{\alpha'}|}{a_\gamma}$ along $\langle\bar{1}10\rangle_{FCC}$ is needed to achieve the correct shape. This is illustrated in Fig. 1 (a), showing atoms in $(111)_{FCC}||(110)_{BCC}$ (red) shuffle by $\frac{\delta a_\gamma}{\sqrt{2}}[\bar{1}10]_{FCC}$ (orange arrows) to reach the correct BCC shape (green). The principal strains to compute γ_T are [8]: $\eta_1 = \frac{\frac{1}{\sqrt{2}}a_\gamma(1-\frac{\delta}{\sqrt{2}})-a_{\alpha'}}{\frac{1}{\sqrt{2}}a_\gamma(1-\frac{\delta}{\sqrt{2}})}$, $\eta_2 = \frac{\frac{1}{\sqrt{2}}a_\gamma(1+\frac{\delta}{\sqrt{2}})-a_{\alpha'}}{\frac{1}{\sqrt{2}}a_\gamma(1+\frac{\delta}{\sqrt{2}})}$ and $\eta_3 = \frac{\frac{1}{\sqrt{2}}a_\gamma-a_{\alpha'}}{\frac{1}{\sqrt{2}}a_\gamma}$. The transformation strain is: $\gamma_T = \sqrt{\eta_1^2+\eta_2^2+\eta_3^2}$. The principal strains of

[1] These are idealised relations, however they have shown sufficient accuracy with experiments when determining various crystallographic parameters [5–7].

E-mail address: eg375@cam.ac.uk (E. Galindo-Nava).

http://dx.doi.org/10.1016/j.scriptamat.2017.05.026
1359-6462/

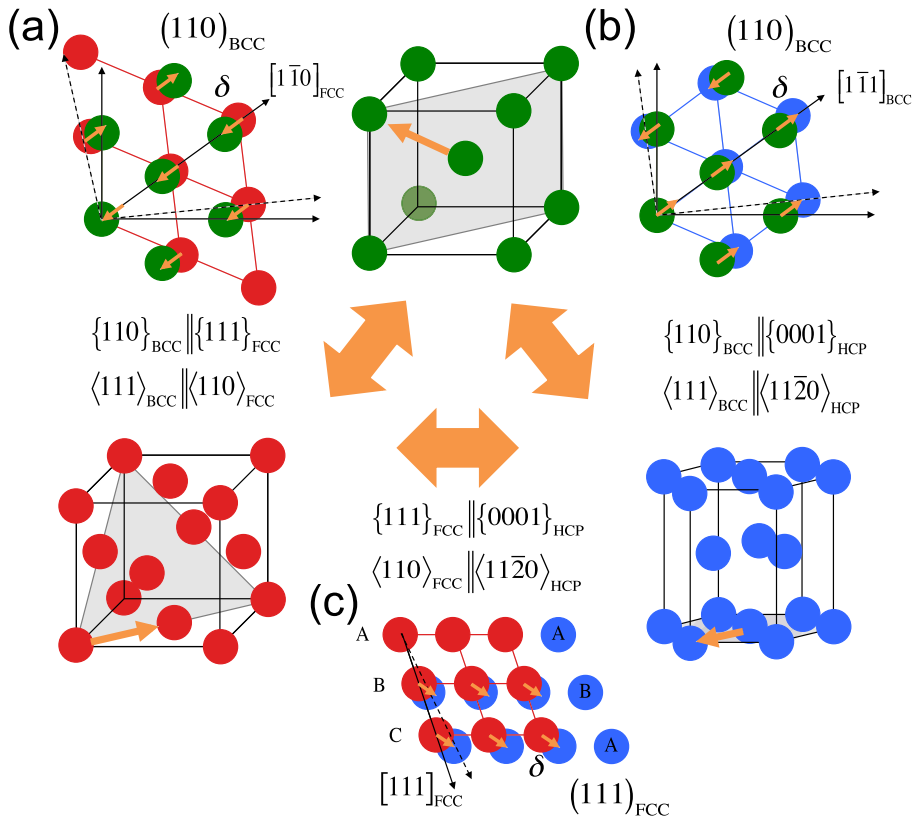

Fig. 1. Schematic representation of the atomic displacements in BCC⟺FCC, FCC⟺HCP and BCC⟺HCP transitions and their orientation relationships. (For interpretation of the references to color in this figure, the reader is referred to the web version of this article.)

the BCC⇒FCC transition are computed by similar rotations and by shearing $\frac{\delta a_{\alpha'}}{\sqrt{3}}[1\bar{1}1]_{BCC}$ the lattice, with $\delta = \frac{|\sqrt{2}a_\gamma - \sqrt{3}a_{\alpha'}|}{a_{\alpha'}}$.

Burgers [9] followed a similar argument to compute γ_T in the BCC⇒HCP transition. This is illustrated in Fig. 1 (b), where BCC atoms shear $\delta = \frac{|\sqrt{3}a_\beta - 2a_\alpha|}{a_\beta}$ along $\langle 111\rangle_{BCC}$ to achieve the correct shape of the HCP lattice (blue atoms). The shifting of $\frac{\delta a_{\alpha'}}{\sqrt{3}}[1\bar{1}1]_{BCC}$ in the BCC axes is included in the computation of the principal (Bain) strains [10].

The FCC⇒HCP transformation strain is obtained by shearing atoms $\delta = \frac{1}{6}\langle 11\bar{2}\rangle$ [11–14]. Two of the principal strains (η_1 and η_2) are obtained by rotating and expanding $[100]_{FCC}$ and $[010]_{FCC}$ in correspondence with $[10\bar{1}0]_{HCP}$ and $[11\bar{2}0]_{HCP}$ [14]. As for η_3, the $[111]_{FCC}$ axis is expanded by δ to lie parallel to $[0001]_{HCP}$, as schematically shown in Fig. 1 (c) (orange arrows). This results in its magnitude increasing to $a_\gamma\sqrt{\left(1+\frac{1}{6}\right)^2+\left(1+\frac{1}{6}\right)^2+\left(1-\frac{2}{6}\right)^2} = a_\gamma\sqrt{\frac{19}{6}}$ and η_3 is [14]: $\eta_3 = \frac{\frac{2}{3}\sqrt{\frac{19}{6}}a_\gamma - c_\epsilon}{\frac{2}{3}\sqrt{\frac{19}{6}}a_\gamma}$. The HCP⇒FCC transition has been argued to occur by the reverse process with analogous principal strains [13,14].

Table 1 shows the values of the principal strains and the resulting transformation strains. The lattice constants have been obtained from Refs. [7,15-18]; these are for Fe $a_\gamma = 0.357$ nm and $a_\alpha = 0.287$ nm; for Ti, $a_\beta = 0.328$ nm, $a_\alpha = 0.295$ nm and $c_\alpha = 0.468$ nm; and for Co, $a_\gamma = 0.35$ nm, $a_\epsilon = 0.25$ nm and $c_\epsilon = 0.406$ nm.

The chemical driving force for athermal martensite, $\Delta G^{\gamma\Rightarrow\alpha'}$, is the difference of the Gibbs energy between the austenite and the martensite. $\Delta G^{\gamma\Rightarrow\alpha'}$ has been the subject of extensive investigations in binary and multicomponent alloys combining the CALPHAD (Calculation of phase diagrams) approach and experimental data [21,23,24]; in this context, martensite is treated as supersaturated ferrite in Fe [24], and supersaturated α in Ti and

Table 1
Transformation strain and ΔG_T in different phase transitions.

Transition	η_1	η_2	η_3	γ_T	$\lvert\Delta G_T\rvert$ (J/mol)	Exp (J/mol)
FCC⇒BCC	$\frac{\frac{1}{\sqrt{2}}a_\gamma(1+\frac{\delta}{\sqrt{2}})-a_{\alpha'}}{\frac{1}{\sqrt{2}}a_\gamma(1+\frac{\delta}{\sqrt{2}})}$	$\frac{\frac{1}{\sqrt{2}}a_\gamma(1-\frac{\delta}{\sqrt{2}})-a_{\alpha'}}{\frac{1}{\sqrt{2}}a_\gamma(1-\frac{\delta}{\sqrt{2}})}$	$\frac{\frac{1}{\sqrt{2}}a_\gamma-a_{\alpha'}}{\frac{1}{\sqrt{2}}a_\gamma}$	0.24 (Fe)	1255	1000–1250 [19–21]
BCC⇒FCC	$\frac{a_{\alpha'}(1+\frac{\delta}{\sqrt{3}})-\frac{\sqrt{2}}{2}a_\gamma}{a_{\alpha'}(1+\frac{\delta}{\sqrt{3}})}$	$\frac{\sqrt{2}a_{\alpha'}(1-\frac{\delta}{\sqrt{3}})-\sqrt{\frac{3}{2}}a_\gamma}{\sqrt{2}a_{\alpha'}(1-\frac{\delta}{\sqrt{3}})}$	$\frac{\sqrt{2}a_{\alpha'}(1+\frac{\delta}{\sqrt{3}})-\sqrt{\frac{3}{2}}a_\gamma}{\sqrt{2}a_{\alpha'}(1+\frac{\delta}{\sqrt{3}})}$	0.17 (Fe)	500	
BCC⇒HCP	$\frac{(1+\frac{\delta}{\sqrt{3}})a_\beta-a_{\alpha'}}{(1+\frac{\delta}{\sqrt{3}})a_\beta}$	$\frac{(1-\frac{\delta}{\sqrt{3}})\sqrt{2}a_\beta-\sqrt{3}a_{\alpha'}}{(1-\frac{\delta}{\sqrt{3}})\sqrt{2}a_\beta}$	$\frac{(1+\frac{\delta}{\sqrt{3}})\sqrt{2}a_\beta-c_{\alpha'}}{(1+\frac{\delta}{\sqrt{3}})\sqrt{2}a_\beta}$	0.1014 (Ti)	130	150 [3]
FCC⇒HCP	$\frac{\frac{1}{\sqrt{2}}a_\gamma-a_\varepsilon}{\frac{1}{\sqrt{2}}a_\gamma}$	$\frac{\frac{1}{\sqrt{2}}a_\gamma-a_\varepsilon}{\frac{1}{\sqrt{2}}a_\gamma}$	$\frac{\frac{2}{3}\sqrt{\frac{19}{6}}a_\gamma-c_\varepsilon}{\frac{2}{3}\sqrt{\frac{19}{6}}a_\gamma}$	0.026 (Co)	18	35 [22]
HCP⇒FCC	$\frac{\sqrt{2}a_\varepsilon-a_\gamma}{\sqrt{2}a_\varepsilon}$	$\frac{\sqrt{2}a_\varepsilon-a_\gamma}{\sqrt{2}a_\varepsilon}$	$\frac{c_\varepsilon-\frac{2}{3}\sqrt{\frac{19}{6}}a_\gamma}{c_\varepsilon}$	0.027 (Co)	18.8	